Appl. Sci. Converg. Technol. 31 (5); 110-112 (2022)
https://doi.org/10.5757/ASCT.2022.31.5.110
eISSN: 2288-6559

Research Paper Check for updates

Electron Tunneling Enhancement in MoS_2/Hexagonal Boron Nitride/Multilayer Graphene Heterostructures by Bubble Formation

Received 29 August, 2022; accepted 15 September, 2022

Oh Hun Gwon[a], Seo Gyun Jang[a], Jong Yun Kim[b], Han Seul Kim[c], and Young-Jun Yu[a,b,*]

[a]Department of Physics, Chungnam National University, Daejeon 34134, Republic of Korea
[b]Institute of Quantum Systems, Chungnam National University, Daejeon 34134, Republic of Korea
[c]Center for Supercomputing Applications, National Institute of Supercomputing and Networking, Korea Institute of Science and Technology Information, Daejeon 34141, Republic of Korea

*Corresponding author E-mail: yjyu@cnu.ac.kr

ABSTRACT

Unintentional bubbles are formed when manufacturing devices using two-dimensional materials. Usually, these bubbles affect device performance degradation, but in the case of memory devices, an additional charge trap can be expected. We investigate the direct surface potential of bubbles formed in a hexagonal boron nitride (hBN)/multilayer graphene (MLG) heterostructure. Specifically, we study the electron transfer improvement by increasing the memory window of a MoS_2/hBN/MLG heterostructure in floating gate memory owing to bubbles formed at the hBN/MLG heterointerface. This characterization of bubbles containing molecules such as water or hydrocarbon in two-dimensional material heterointerfaces can promote the understanding of charge carrier tunneling in two-dimensional material heterostructures.

Keywords: Heterostructure, Floating Gate Memory, Memory Window, Bubble

1. Introduction

Floating gate memory (FGM)-based two-dimensional (2D) material heterostructures can achieve high performance and stability [1–9]. For instance, the transition-metal dichalcogenide (TMDC) semiconductor channel, hexagonal boron nitride (hBN) dielectric layer, and multilayer graphene (MLG) semimetal layer heterostructure have been demonstrated and widely used in FGM devices [1–9]. The program and erase steps in memory can be achieved by electron tunneling between the TMDC channel and MLG heterostructure through the hBN barrier. Hence, the tunneling condition of hBN in a TMDC/hBN/MLG heterostructure is important in FGM applications [1–9].

For preparing 2D material heterostructures, each layer of 2D material is stacked using micro-transfer systems in air, causing unintended residues in the stacked layer heterointerfaces [10–16]. Such residues are commonly referred to as bubbles. Previous studies on bubbles have considered their influence on tunneling [17–24], and we have previously reported the charge trap by bubble formation in a TMDC/hBN/MLG heterointerface [9]. We observed the tunneling carrier density through the hBN area that includes bubble formation and analyzed an additional charge trapping layer for electron transfer between TMDC and MLG layers in TMDC/hBN/MLG heterostructures.

In the present study, we characterized the surface potential variation on the bubble area at an hBN/MLG heterointerface. Using a MoS_2/hBN/MLG heterostructure FGM device, we confirmed that the electron transfer ratio enhances the memory window (MW) for bubbles formed at the hBN/MLG heterointerface compared with a flat interface area. This characterization of electron tunneling behavior for bubbles in 2D material heterointerfaces may unveil properties of real electron tunneling in 2D material heterostructures for charge carrier tunneling devices with unintended residues.

2. Experimental details

Figure 1 shows the fabrication steps of the MoS_2/hBN/MLG heterostructure on a SiO_2 substrate using a micro-transfer system [25–28]. A 40-nm-thick hBN dielectric layer was stacked on MLG (22 nm in thickness), which was initially prepared on a 280-nm-thick SiO_2 substrate by mechanical exfoliation. Then, multilayer MoS_2 (26 nm in thickness) was transferred to hBN/MLG/SiO_2, as illustrated in Figs. 1(a)-(c). During transfer, we observed the formation of bubbles, as shown in Figs. 1(b) and 1(c). To verify the surface doping variation owing to bubble formation in MoS_2/hBN/MLG heterostructures, we performed scanning Kelvin probe microscopy (SKPM) using a commercial atomic force microscope (XE-100; Park Systems, Suwon, Korea) in air at room temperature. To investigate the spatial surface potentials on the surface of 2D material heterostructures, we used the feedback process (measuring contact potential difference V_{CPD}) under applied AC voltage of ~1 V, DC voltage of 0.5 V, and frequency of 17 kHz to an Au-coated probe.

3. Results and discussion

Figure 2 shows the spatial distribution of the contact potential difference for the MoS_2/hBN/MLG surface including bubbles. Owing to

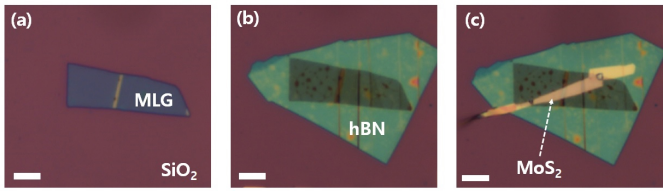

Figure 1. Optical images of MoS_2/hBN/MLG stacking. (a) Image of mechanically exfoliated MLG on SiO_2 substrate. (b) Image of hBN stacked on MLG/SiO_2 substrate. (c) Image of MoS_2 stacked on hBN/MLG/SiO_2 substrate (Scale bars, 10 μm).

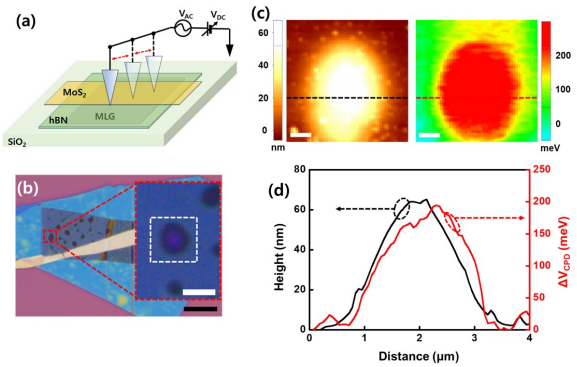

Figure 2. (a) Schematic diagram of SKPM applied to MoS_2/hBN/MLG heterostructure. (b) Optical image of MoS_2/hBN/MLG heterostructure (scale bar, 10 μm). Inset: enlarged image of a bubble on MoS_2 surface (scale bar, 2 μm). (c) Topography (left) and surface potential (right) images of bubble shown in inset of panel b (scale bars, 0.5 μm). (d) Height (black line) and $\triangle V_{CPD}$ (red line) profiles following dashed lines for topography and surface potential image shown in panel c.

the increasing influence of bubbles at the 2D heterostructure, we chose a large bubble with 60 nm in height [Figs. 2(a) and 2(b)] for analysis. To confirm bubble doping, we evaluated the normalized contact potential ($\triangle V_{CPD}$) considering a flat hBN area as reference (i.e., $\triangle V_{CPD}$ = 0 meV), as shown in Fig. 2(c). $\triangle V_{CPD} \approx$ 200 meV at the center of bubble region [Fig. 2(d)], indicating doping variation by the formation of bubbles in hBN/MLG heterostructures. This $\triangle V_{CPD}$ value can be attributed to molecules trapped in bubbles at the hBN/MLG interface. The tunneled carrier density has shown enhancement through hBN from MLG to MoS_2 layers in MoS_2/hBN/MLG heterostructures by residues such as water or hydrocarbon (i.e., bubbles) [9].

To investigate electron tunneling related to bubble formation between hBN and MLG, we connected Cr/Au (10/100 nm in thickness) electrodes to an MoS_2 channel by electron-beam lithography, as shown in Fig. 3. We chose two regions covering bubble [A1 in Fig. 3(a)] and flat [A3 in Fig. 3(a)] areas on the hBN/MLG heterostructure and transferred a MoS_2 layer covering both areas. Employing the electrode marked by E2 as border, the electric transport characterization was investigated by measuring the drain-source current (I_{DS}) for V_{12} = 0.1 V (red scheme between E1 and E2) and V_{23} = 0.1 V (blue scheme between E2 and E3) according to V_{BG}, as shown in Fig. 3(b). The resulting MoS_2/hBN/MLG heterostructure was employed as a memory device with electron transfer between the MLG and MoS_2 layers, leading to hysteresis in the transport curves for the MoS_2 channel according to the forward (+) and backward (–) sweeps of V_{BG}. We considered the hysteresis as the MW [9,29].

The hysteresis for transport curves (I_{DS} vs. V_{BG} for V_{12}) on the bubble-containing MoS_2 channel area [Fig. 3(d)] was larger than that (I_{DS} vs. V_{BG} for V_{23}) on the flat area [Fig. 3(c)]. Hysteresis in the transport curve for V_{23} while applying forward and backward V_{BG} = ±10 - ±20 V was not observed (i.e., MW « 0.1 V) [Fig. 3(c)]. On the other hand, the opened MW for V_{BG} = ±30 V was observed with approxi-

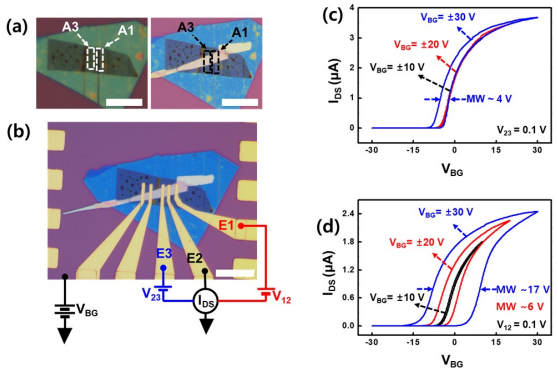

Figure 3. (a) Optical image before (left) and after (right) transferring MoS_2 to hBN/MLG. Clean and bubble-containing areas at hBN/MLG interface enclosed by black dashed boxes with A3 and A1, respectively. (Scale bars, 20 μm) (b) Optical image of Au electrodes connected to MoS_2/hBN/MLG heterostructure FGM. Characterization conductance with V_{12} (red line between E1 and E2) or V_{23} (blue line between E2 and E3) according to V_{BG}. (Scale bar, 20 μm) (c) Current variation (I_{DS}) with bias voltage V_{12} between E1 and E2 according to V_{BG}. (d) Current variation (I_{DS}) with bias voltage V_{23} between E2 and E3 according to V_{BG}.

mately 4 V. Hence, electron tunneling through hBN between the MoS_2 and MLG layers began for V_{BG} larger than ±30 V. For the bubble-containing MoS_2 channel area [Fig. 3(d)], the MW was much smaller than 0.1 V for ±10 V, but the MW opened 6 V for ±20 V and 17 V for ±30 V. This indicates that tunneled electrons between MoS_2 and MLG are enhanced by bubble formation between hBN and MLG. Therefore, bubble formation on the surface interface in TMDC/hBN/MLG heterostructures can allow to change the direct surface potential variation and transport characteristics by trapped charges.

4. Conclusion

We characterized the effects of bubbles formed at hBN/MLG interfaces on the electron tunneling ratio of a MoS_2/hBN/MLG heterostructure. Evidence of charge trapping was obtained from direct observation by SKPM of the surface potential variation by doping changes on a bubble-containing area at the hBN/MLG heterointerface. Based on measurements of the MW enhancement for a MoS_2/hBN/MLG FGM device with bubbles formed at the hBN/MLG interface, we confirmed the trapped charges by bubble formation leading to improved electron tunneling ratio between the MoS_2 channel and MLG floating gate layer. This result may contribute to understanding the role of trapped molecules in bubbles formed on 2D material heterostructures for electron tunneling applications.

Acknowledgments

This work was supported by the research fund of Chungnam National University.

Conflict of Interest

The authors declare no conflicts of interest.

ORCID

Oh Hun Gwon https://orcid.org/0000-0003-2633-7077
Seo Gyun Jang https://orcid.org/0000-0003-2466-8358
Jong Yun Kim https://orcid.org/0000-0002-2161-8972
Han Seul Kim https://orcid.org/0000-0003-0731-6705
Young-Jun Yu https://orcid.org/0000-0001-9446-1526

References

[1] A. A. Bessonov, M. N. Kirikova, D. I. Petukhov, M. Allen, T. Ryhänen, and M. J. A. Bailey, Nature Mater. 14, 199 (2015).

[2] M. Wang *et al.*, Nat. Electron. 1, 130 (2018).
[3] A. J. Hong *et al.*, ACS Nano 5, 7812 (2011).
[4] S. Lei *et al.*, Nano Lett. 15, 259 (2015).
[5] Y.-J. Doh and G.-C. Yi, Nanotechnology 21, 105204 (2010).
[6] M. S. Choi, G.-H. Lee, Y.-J. Yu, D.-Y. Lee, S. H. Lee, P. Kim, J. Hone, and W. J. Yoo, Nat. Commun. 4, 1624 (2013).
[7] S. Bertolazzi, D. Krasnozhon, and A. Kis, ACS Nano 7, 3246 (2013).
[8] D. Qiu, D. U. Lee, K. S. Lee, S. W. Park, and E. K. Kim, Nano Res. 9, 2319 (2016).
[9] O. H. Gwon *et al.*, Adv. Funct. Mater. 31, 2105472 (2021).
[10] D.-G. Kim, S. Lee, and K. Kim, Appl. Microsc. 50, 28 (2020).
[11] A. Jain, P. Bharadwaj, S. Heeg, M. Parzefall, T. Taniguchi, K. Watanabe, and L. Novotny, Nanotechnology 29, 265203 (2018).
[12] B. Alemán *et al.*, ACS Nano 4, 4762 (2010).
[13] G. Algara-Siller, O. Lehtinen, A. Turchanin, and U. Kaiser, Appl. Phys. Lett. 104, 153115 (2014).
[14] A. L. Briseno, M. Roberts, M.-M. Ling, H. Moon, E. J. Nemanick, and Z. Bao, J. Am. Chem. Soc. 128, 3880 (2006).
[15] S.-M. Kim, C.-K. Lee, S.-U Yoon, K.-S. Kim, and Y. Hwangbo, Nanotechnology 33, 165301 (2022).
[16] S. Shin, S. Kim, T. Kim, H. Du, K. S. Kim, S. Cho, and S. Seo, Carbon 111, 215 (2017).
[17] R. Villarreal *et al.*, Nano Lett. 21, 8103 (2021).
[18] Z. Qi, A. L. Kitt, H. S. Park, V. M. Pereira, D. K. Campbell, and A. H. Castro Neto, Phys. Rev. B 90, 125419 (2014).
[19] P. Jia *et al.*, Nat. Commun. 10, 3127 (2019).
[20] J. Lu, A. H. Castro Neto, and K. P. Loh, Nat. Commun. 3, 823 (2012).
[21] N. Levy, S. A. Burke, K. L. Meaker, M. Panlasigui, A. Zettl, F. Guinea, A. H. Castro Neto, and M. F. Crommie, Science 329, 544 (2010).
[22] S. J. Haigh *et al.*, Nature Mater. 11, 764 (2012).
[23] Y. Xiao, Z. Cui, S. Zhou, M. Li, J. Li, F. Luo, M. Zhu, Z. Zhu, and S. Qin, J. Phys. Chem. C 126, 13785 (2022).
[24] K. Yue, W. Gao, R. Huang, and K. M. Liechti, J. Appl. Phys. 112, 083512 (2012).
[25] H. K. Choi *et al.*, ACS Appl. Mater. Interfaces 14, 23617 (2022).
[26] J. Y. Kim, O. H. Gwon, S.-J. Kang, H. R. Byun, and Y.-J. Yu, Appl. Sci. Converg. Technol. 30, 78 (2021).
[27] S.-J. Kang *et al.*, Adv. Funct. Mater. 24, 5157 (2014).
[28] O. H. Gwon, J. Y. Kim, S.-J. Kang, and Y.-J. Yu, Appl. Sci. Converg. Technol. 29, 180 (2020).
[29] N. Zagni, P. Pavan, and M. A. Alam, Appl. Phys. Lett. 117, 152901 (2020).